scientific reports

Check for updates

OPEN

Microwave assisted synthesis and bioactive potential of folic acid functionalized tellurium nanoparticles (FA@Te NPs) against HeLa cancer cells

Naghmeh Satarzadeh[1,2], Soudabe Riahi-Madvar[2,3], Mojtaba Shakibaie[6]✉, Mahboubeh Adeli-Sardou[4]✉, Hamid Forootanfar[1] & Farzaneh Jabari Morouei[5]

Chemotherapy is currently one of the most effective treatments for cancer, but it is often accompanied by nonspecific toxicity and drug resistance. Nanostructures, particularly tellurium-based ones, have anticancer potential, but further research is needed to determine their biological activities. Adding targeting molecules to such nanoparticles, such as folic acid, may increase their efficacy and selectivity. This study focused on the synthesis of folic acid-incorporated tellurium nanoparticles (FA@Te NPs) using a microwave-assisted method involving a K_2TeO_3 solution (1 mM) with $NaBH_4$ and folic acid. The synthesized nanoparticles were analyzed using various techniques such as UV-visible spectroscopy, scanning electron microscopy (SEM), energy dispersive X-ray spectroscopy (EDS), X-ray diffraction (XRD), and Fourier transform infrared spectroscopy (FTIR). The nanoparticles, predominantly hexagonal and ranging in size from 3.9 nm to 11 nm, were then subjected to in vitro tests to assess their antioxidant activities, hemocompatibility, and cytotoxic effects. The FA@Te NPs demonstrated superior DPPH scavenging activity compared to bare Te NPs across concentrations from 20 µg/mL to 1280 µg/mL. Hemolytic tests revealed that FA@Te NPs had a significantly higher hemolytic potential than Te NPs at concentrations between 20 and 40 µg/mL. The IC50 values for HeLa cells treated with FA@Te NPs, Te NPs, and Cisplatin for 24 h were found to be 767.6 ± 8.8 µg/mL, 1399.5 ± 5.2 µg/mL, and 142.7 ± 4.6 µg/mL, respectively. Exposure to IC50 concentrations of FA@Te NPs and Te NPs resulted in a significant increase in necrosis and late-stage apoptosis in HeLa cells, highlighting the strong cytotoxicity of these nanoparticles. Further research is needed to understand the biological mechanisms underlying the activities of FA@Te NPs.

Keywords Tellurium nanoparticles containing folic acid, Microwave irradiation, Antioxidant, Hemocompatibility, Cytotoxicity

Tellurium (Te), a metalloid element, is known to exist in multiple allotropic forms and commonly exhibits oxidation states of − 2, + 4, and + 6. Its unique properties make it valuable in several industries. It is commonly used to manufacture alloys, glass, and solar panels. One notable use of tellurium is in creating thin films with semiconducting properties, enabling solar panels to transform sunlight into electricity effectively. Sensors based on tellurium are used in a variety of industries for environmental monitoring and gas detection processes[1]. Among the trace elements in the average human body, tellurium is the fourth most abundant, with about 0.7

[1]Pharmaceutical Sciences and Cosmetic Products Research Center, Institute of Pharmaceutical Sciences, Kerman University of Medical Sciences, Kerman, Iran. [2]Department of Pharmaceutical Biotechnology, Faculty of Pharmacy, Kerman University of Medical Sciences, Kerman, Iran. [3]The Student Research Committee, Faculty of Pharmacy, Kerman University of Medical Sciences, Kerman, Iran. [4]Department of Biotechnology, Institute of Science and High Technology and Environmental Sciences, Graduate University of Advanced Technology, Kerman, Iran. [5]Department of Medical Laboratory Sciences, Faculty of Paramedical Sciences, Tehran Medical Sciences Branch, Islamic Azad University, Tehran, Iran. [6]Herbal and Traditional Medicines Research Center, Institute of Pharmaceutical Sciences, Kerman University of Medical Sciences, Kerman, Iran. ✉email: shakiba@kmu.ac.ir; adeli.mahboubeh@gmail.com

mg (after iron, zinc, and lead)[2]. Tellurium compounds have been used to treat various bacterial infections such as *Escherichia coli*, *Pseudomonas aeruginosa*, *Staphylococcus aureus*, *Mycobacterium leprae*, *M. tuberculosis* cystitis, and eye infections[3–5]. Recent research indicates that these compounds possess additional biological properties, such as the capacity to decrease cytokine production in T cells[6], regulate the immune system[7], inhibit the sickling of red blood cells[8], and have anticancer potentials[9]. Nevertheless, these drugs do not selectively target cancer cells, thus causing toxic side effects for normal cells[10]. Given the drawbacks and various side effects of conventional tellurium-based compounds, there is an increasing interest in developing new tellurium compounds or alternative administration methods to alleviate these side effects[11]. As nanotechnology has developed in medicine, nanomedicine has provided novel solutions for treating a variety of cancers, including tailored medication delivery techniques that might be able to eradicate tumors without damaging healthy tissues[10]. Additionally, chalcogens like tellurium (Te) and selenium (Se) are becoming increasingly popular in nanomedicine for biological uses[12].

The unique structure of Tellurium nanoparticles (Te NPs) makes them an attractive option for modern applications. For example, Tellurium-based quantum dots display fluorescence properties, making them efficient as biological markers[13]. The use of tellurium nanomaterials in tumor photodynamic therapy, synergetic therapy, photothermal therapy, photo-triggered molecule delivery, and tumor phototherapy has been documented[14]. Recently, the utility of tellurium has been enhanced through the use of Copper telluride nanocubes[15], Hybrid tellurium–lignin nanoparticles[16], osmium–osmium–tellurium nanozymes[17], cantharidin-tellurium nanoparticles[18], and bifunctional tellurium nanodots[19].

In recent years, researchers have noticed that surface coatings have become a crucial innovation to address issues that uncoated nanoparticles encounter, including poor targeting, nonspecific toxicity, aggregation, and quick immune system clearance[20,21].

Folic acid (FA), also referred to as vitamin B9, is an essential nutrient required for synthesizing DNA and RNA, producing methionine, activating vitamin B12, and cell division and growth[22]. The Folate receptor (FR) family, also known as membrane folate-binding proteins, has a high affinity for folic acid and its reduced derivatives, facilitating the transport of 5-methyltetrahydrofolate into cells[23]. FRs are overexpressed in several malignancies, such as breast, ovary, lung, colon, kidney, head and neck, brain, and myeloid cancers, while their presence in normal tissues is limited and typically low-level. This selective overexpression makes FRs excellent targets for cancer imaging and therapy, because treatments or imaging agents directed toward FRs can preferentially bind to tumor cells over normal cells, improving detection and treatment specificity[24–26]. Nanomaterials containing folic acid have recently been developed through various approaches to improve their uptake by folate receptor (FR)-positive cancer cells, offering a promising strategy for targeted cancer therapy. These FA-linked nanomaterials exploit the high expression of folate receptors—especially FRα—in many tumors to achieve selective delivery of therapeutic agents directly to cancer cells, enhancing treatment efficacy while minimizing side effects on normal tissues[27,28].

Being folate receptor-positive, HeLa cells provide a valuable model for investigating ligand-mediated targeting strategies that exploit the high selectivity and affinity of folate receptors for targeted drug delivery[23]. Understanding the behavior of HeLa cells as folate receptor-positive cells sheds light on the mechanisms of cellular uptake and opens up possibilities for developing more effective and targeted cancer therapies[29].

Microwaves (MW), a form of electromagnetic radiation with frequencies ranging from 300 MHz to 300 GHz, are widely used as a novel heating method in various fields today[30]. The use of MW in the preparation of nanostructures offers several benefits, including the production of nanomaterials with high purity and a narrow size distribution[31]. Additional advantages of MW irradiation, such as reduced energy consumption, consistent heating, and uniform nucleation and growth of nanoparticles, make it ideal for the preparation of various nanoparticles[32]. This study presents a new, quick, and straightforward method for the microwave-assisted synthesis of FA@Te NPs. Following the evaluation of the physicochemical properties of the prepared NPs, their antioxidant and hemolytic properties, as well as their cytotoxic effects on HeLa cells, were also examined.

Materials and methods

Chemicals

The chemicals utilized in this study were obtained from Sigma Company (St. Louis, MO, USA) and included sodium borohydride, folic acid, potassium tellurite (K_2TeO_3), and 3-(4, 5-dimethylthiazol-2-yl)-2, 5-diphenyl-2 H-tetrazolium bromide (MTT). Additional reagents, including 2,2-diphenyl-1-picrylhydrazyl (DPPH), disodium hydrogen phosphate (Na_2HPO_4), sodium dihydrogen phosphate (NaH_2PO_4), sodium carbonate (Na_2CO_3), potassium ferricyanide, trichloro acetic acid (TCA), dextrose, ascorbic acid, citric acid, sodium citrate, and ferric chloride ($FeCl_3$) were supplied by Merck (Germany). Borna Pouyesh Gene Company (BPGene Co., Kerman, Iran) provided fetal bovine serum and DMEM medium.

Preparation of NPs

For the synthesis of FA@Te NPs, a solution of 200 µL of 0.1 mM folic acid was combined with 5 mL of 1 mM K_2TeO_3. This mixture was then treated with 1 mL of ice-cold sodium borohydride solution (1 mg/mL) and subjected to three microwave irradiation cycles, each consisting of 30 s of irradiation at 850 W and 30 s of rest, leading to a color change to dark black. The suspension was centrifuged at 12,000 rpm for 15 min, and the resulting pellet was rinsed thrice with deionized water. The same procedure was followed for the preparation of tellurium nanoparticles, excluding the use of folic acid. The nanoparticle stock was sterilized by autoclaving for 20 min at 200 kPa and 121 °C[33].

Characterization of NPs

Various techniques and instruments were employed to characterize Te NPs and FA@Te NPs. The UV spectrum of Folic acid, Te NPs, and FA@ Te NPs was recorded in the 200–400 nm range using a UV-Vis. Spectrophotometer (UV-1800, Shimadzu Co., USA). A scanning electron microscope (Zeiss 902 A) equipped with an energy-dispersive X-ray (EDX) microanalyzer was used to capture SEM images of NPs and perform their elemental analysis. The particle size distribution patterns of the synthesized nanostructures were determined using a Zetasizer MS2000 (Malvern Instruments, Malvern, UK). In addition, the crystalline structure of NPs was examined using an X-ray diffractometer (Philips X'Pert-MPD) with CuKa radiation (k = 1.5405 Å), within the range of 20°–80°. The corresponding XRD spectrum was further analyzed with High Score Plus software (Version 5.2). The FTIR spectrum of oven-dried NPs was obtained at 400–4000 cm^{-1} using a NicoletTM iS20 FTIR spectrophotometer. A spectrophotometric method was used for quantitative analysis. The standard curve of folic acid was initially established by comparing the absorbance measured at 285 nm to various concentrations of Folic acid (1–25 μg mL^{-1}) dissolved in water. Subsequently, the freshly prepared suspension of FA@Te nanoparticles was centrifuged (11,000 rpm, 20 min), and the UV absorbance of the supernatant was measured at 285 nm against the supernatant of a freshly prepared Te NPs suspension prepared using the same method but without Folic acid. Different NPs were prepared on various days for the three procedures. After determining the dry weight of FA@Te NPs (50 °C, 48 h), the average of the measured absorbance was used to quantify the amount of folic acid on the NPs surface[33].

Evaluating the antioxidant properties of NPs

DPPH scavenging activity

The ability of FA@Te NPs, Te NPs, and Ascorbic acid to scavenge radicals in aqueous media was assessed by adapting a previous method[34]. Various concentrations (0–1280 μg/mL) were combined with 150 mL of a 1 mM DPPH solution. After a 30-minute incubation period in the dark at room temperature, the absorbance was measured at 517 nm. Deionized water and ascorbic acid solutions (0–1280 mg/mL) were used to establish negative and positive controls, respectively. The percentage of DPPH scavenging activity was calculated using the following formula:

$$\text{DPPH scavenging effect } (\%) = [1 - (\text{Aa} - \text{Ab})/\text{Ac}] \times 100$$

where Aa is the absorbance of the sample mixed with DPPH, Ab is the absorbance of the sample without DPPH, and Ac is the absorbance of the control solution.

Reducing power assay

A refined version of a previously established method was used to measure the reducing power of the NPs[35]. In this method, 500 μL of NPs solutions (0–1280 μg/mL) were mixed with 250 μL of 1% w/v potassium ferricyanide and 250 μL of 0.2 M sodium phosphate buffer. The mixture was then heated at 65 °C for 20 min. Subsequently, 1 mL of 10% w/v TCA solution was added, and the mixture was centrifuged for 15 min at 3000 rpm. The supernatant was combined with 100 μL of deionized water and 20 μL of 6 mM $FeCl_3$. The absorbance of the samples was measured at 700 nm. Ascorbic acid solutions (0–1280 μg/mL) served as a control. A graph was constructed using the mean absorbance values from three experiments conducted in triplicate.

In vitro hemolytic assay

To evaluate the hemolytic properties of the NPs, a previously described method was employed[36]. Whole blood cells were obtained from the Iranian Blood Transfusion Organization (IBTO). All experimental procedures related to the preparation of these whole blood pack cells were carried out following the IBTO guidelines and regulations.

The red blood cells were centrifuged at 3000 rpm for 5 min at 5 °C. Using Alsever's solution (0.1116 M dextrose, 0.071 M sodium chloride, 0.027 M sodium citrate, and 0.002 M citric acid), the RBC pellets were washed thrice and diluted at a 1:10 ratio. The resulting cell suspension was incubated at 37 °C for 30 min with an equal volume of NPs at concentrations varying from 0 to 1280 μg/mL in a shaker incubator[37]. After centrifuging the supernatant for four minutes at 3000 rpm, the supernatant was collected. Deionized water and Alsever's solution were controls (representing 100% hemolysis and 0% hemolysis, respectively). The absorbance of the samples was measured at a wavelength of 415 nm. The experiment was conducted three times on separate days, and the percentage of hemolysis (HP) was calculated using the following formula:

$$\text{HP } (\%) : [(\text{Ap} - \text{An})/(\text{As} - \text{An})] \times 100$$

Where As is the absorbance of the experimental group, An is the absorbance of the negative control group, and Ap is the absorbance of the positive control group.

The Ethics Code Number IR.NIMAD.REC.1403.004 was obtained from the Research Ethics Committee of the Kerman University of Medical Sciences. The hemolysis assay was carried out by the university's established guidelines to ensure ethical and scientific standards were met.

Cytotoxicity test

The HeLa cells (a human breast cancer cell line) were obtained from the Iranian Biological Resource Center. During the logarithmic growth phase, these cells (10^4) were seeded in a 96-well plate. The NPs were added in varying concentrations (0–1280 μg/mL). After 24 h, the medium was replaced with MTT solution and incubated for 3 h. The medium was then replaced with DMSO, and the optical density was measured. The IC_{50} values were

determined using non-linear regression analysis with GraphPad Prism 9 software. The results are presented as the mean ± SD.

Flow cytometry: annexin V-fluorescein isothiocyanate (FITC) and propidium iodide assay

Apoptosis and necrosis were observed using flow cytometry. A total number of 1×10^6 HeLa cells were treated with an inhibitory concentration (IC_{50}) dose of FA@Te NPs and Te NPs for 24 h. Thereafter, the cells were washed with phosphate-buffered saline (PBS), and stained with annexin V-FITC and PI, a DNA dye that distinguishes viable, apoptotic, and late apoptotic or dead cells in flow cytometry, according to the kit's instructions (ApoFlowEx FITC KIT, EXBIO, Czech Republic).

Statistical analysis

To analyze the results of the experiments, a one-way ANOVA was utilized. If the *p*-value was less than 0.05 was considered to be statistically significant.

Results and discussion

Preparation and characterization of NPs

FA@Te NPs were prepared by microwave irradiation of K_2TeO_3 solution containing folic acid in the presence of Sodium borohydride as a reducing agent. Figure 1 exhibited the color of (a) K_2TeO_3 solution (1 mM) containing Folic acid before microwave irradiation, and (b) K_2TeO_3 solution (1 mM) containing Folic acid after microwave irradiation. Furthermore, the UV-Vis absorption spectra of Te NPs, FA@Te NPs, folic acid, and K_2TeO_3 solution were shown in Fig. 1c–e, and f, respectively. Reducing Te ions to Te NPs led to a change in the colorless mixture to dark black. The formation of Te NPs resulted in the elevation of the spectrum (Fig. 1c) compared to the K_2TeO_3 solution (Fig. 1f). Furthermore, FA@Te NPs showed a similar spectrum pattern with the folic acid spectrum (Fig. 1e) with a weak elevation at 285 nm (Fig. 1d). In an earlier study, Forootanfar and colleagues showed that Te NPs, which are rod-shaped and prepared by *P. pseudoalcaligenes* strain Te, have a similar pattern in the UV-visible region between 200 and 400 nm. These nanoparticles are approximately 22 nm in diameter and 185 nm in length[38].

The SEM provided additional information on the morphology and shape of FA@Te nanoparticles (Fig. 2a). The SEM micrograph revealed that the nanoparticles were spherical and had formed larger particles as they interconnected with each other.

The particle size distribution pattern of microwave-assisted synthesized FA@Te NPs showed one peak in the 3.9 to 11 nm size range, with the 6.4 nm size being the most frequent (Fig. 2b). Te NPs had a single peak in the size range of 6 to 11 nm, and 8.8 nm was the most common NP (data not provided).

In a previous study by Phae-Ngam and colleagues, they discovered that the average size of Tellurium nanoparticles (Te NPs), created through long-pulsed laser ablation, varied between 30 and 200 nm[39]. Another study used *Streptomyces graminisoli* for the biosynthesis of Te NPs in the shapes of rods and rosettes, with an average size of 21.4 nm[40]. Tellurium nanoparticles, with a size of 50.1 nm, were also biosynthesized by *Penicillium chrysogenum* PTCC 5031[41]. Additionally, a study reported the production of tellurium nanoparticles using

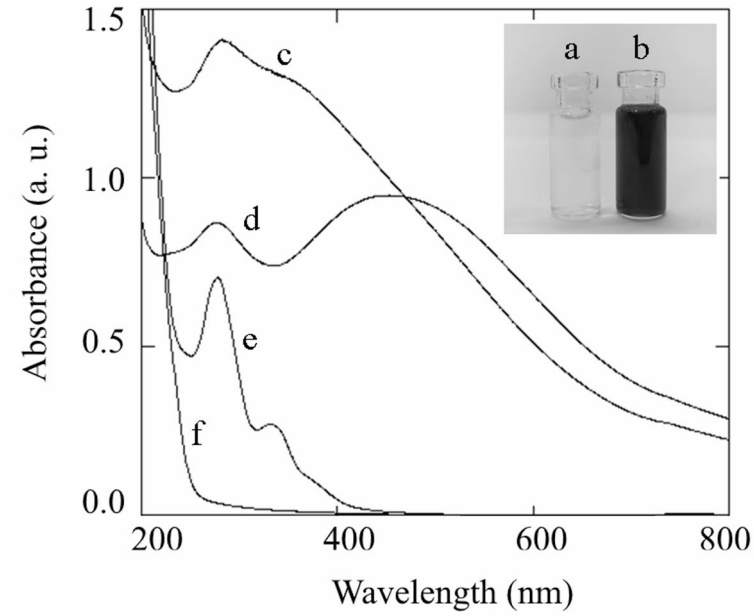

Fig. 1. The reaction mixture's color, consisting of potassium tellurite, Folic acid solution, and sodium borohydride, was observed before (a) and after (b) being heated in a microwave oven. The UV-Vis absorption spectra for (c) Te NPs, (d) FA@Te NPs, (e) Folic acid solution, and (f) potassium tellurite solution.

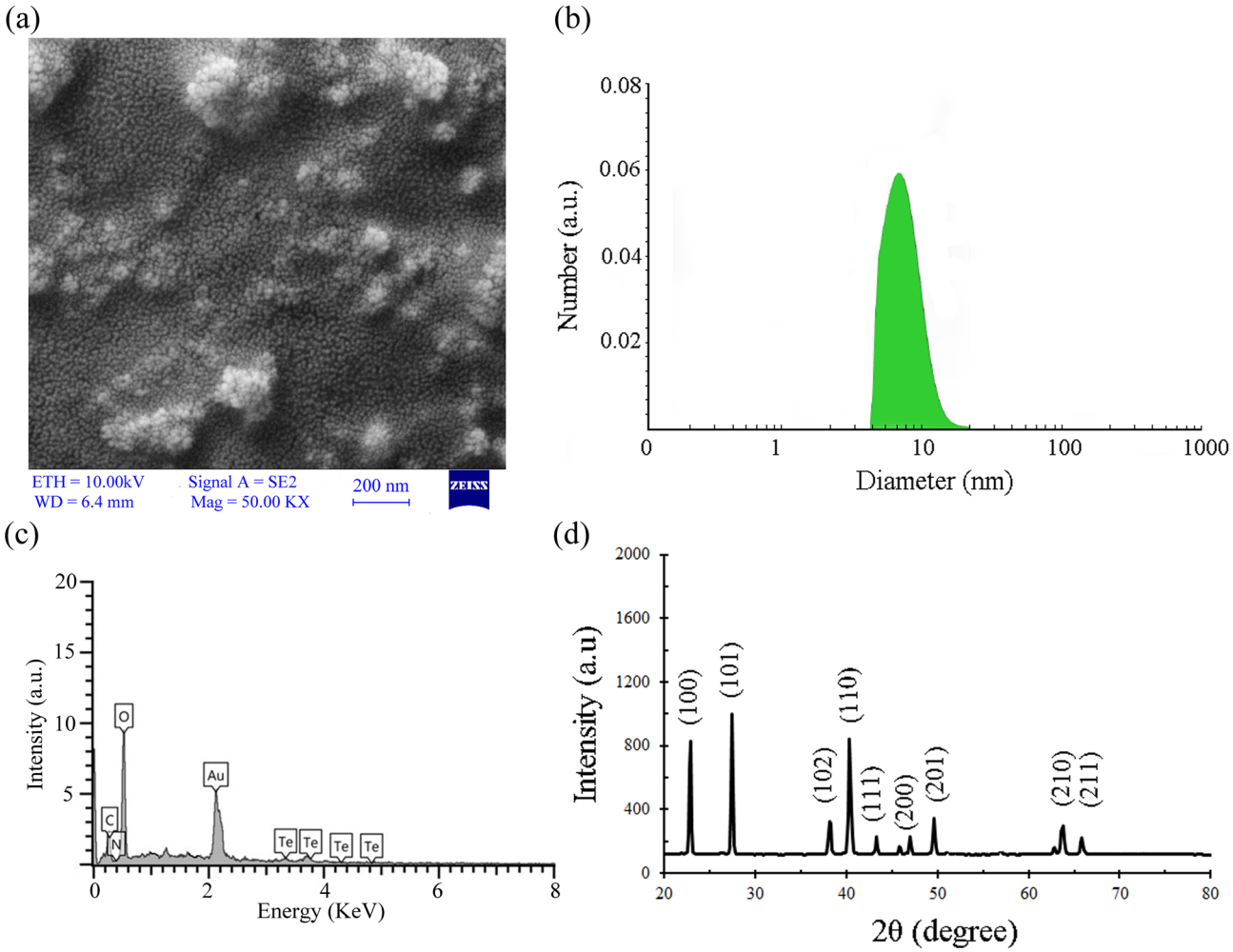

Fig. 2. (a) SEM micrograph, (b) particle size distribution pattern, (c) EDX analysis, and (d) XRD profile of FA@Te NPs prepared by microwave irradiation.

plasma processing, with an average particle size of 100 nm[42]. The variation in size distributions of NPs depends on different synthesis methods.

The EDX profile of the FA@Te NPs displayed peaks of Te Lα at 3.76 keV, which was related to the presence of tellurium in the prepared nanoparticles (Fig. 2c). In the study of Hosseini et al., the existence of tellurium with a similar value of Te Lα (3.76 keV) has been reported in the EDX spectrum of Te nanoparticles (22–148 nm) biosynthesized by Lysinibacillus sp. EBL303[43]. The other three related peaks of carbon Kα (1.28 keV) and spheric Kα (0.52 keV), which were observed in the EDX spectrum (Fig. 2c), could be related to the folic acid in the structure of nanoparticles. Askar et al. also reported similar peaks for C, N, and O in the EDX profile of synthesized Amygdalin-folic acid-nanoparticles[44].

The XRD pattern of FA@Te NPs exhibited (100), (101), (102), (110), (111), (200), (201), (210), and (211) diffraction planes at 2-Theta of 22.8°, 27.4°, 38.15°, 40.4°, 43.3°, 46.96°, 49.6°, 63.7°, and 65.87°, respectively (Fig. 2d). Comparing FA@Te NPs with standard tellurium values (JCPDS 01–078–2312) indicated that they had hexagonal structures with lattice constants a = 4.46 Å, b = 4.46 Å, and c = 5.93 Å. Another study employed a template and surfactant-free electrochemical method at ambient temperature to create Te nanorods. All the similar diffraction peaks were perfectly indexed to the hexagonal structure of tellurium[45]. In addition, Mousavi-Kamazani and colleagues described an easy sonochemical method for the synthesis of hexagonal Te NPs (15–40 nm) that exhibited a similar XRD pattern[46]. Rosales-Conrado et al. synthesized tellurium nanoparticles (10–100 nm) using gallic acid, and XRD analysis revealed that these nanoparticles possess a hexagonal crystal structure[47]. In the present study, both EDX and XRD analyses depicted that Te nanoparticles were successfully obtained via the microwave synthetic route.

FTIR analysis of Folic acid, dried FA@ Te NPs, and Te NPs exhibited several absorption peaks in various regions (Fig. 3). FTIR spectrum of Folic acid (Fig. 3a) exhibited bonds at 3542 cm^{-1}, 3416 cm^{-1}, 2924 cm^{-1}, 1693 cm^{-1}, and 1605 cm^{-1} that could be attributed to N-H, O-H, C-H, C = O, and C = C or C = N stretching vibrations, respectively. FTIR spectrum of FA@Te NPs exhibited absorption peaks at 3421 cm^{-1}, 2922 cm^{-1}, and 2853 cm^{-1}, which could be attributed to O-H, C-H, and stretching vibrations, respectively (Fig. 3b). The microwave-assisted synthesis technique has been effectively employed in the creation of nanostructures, facilitating the

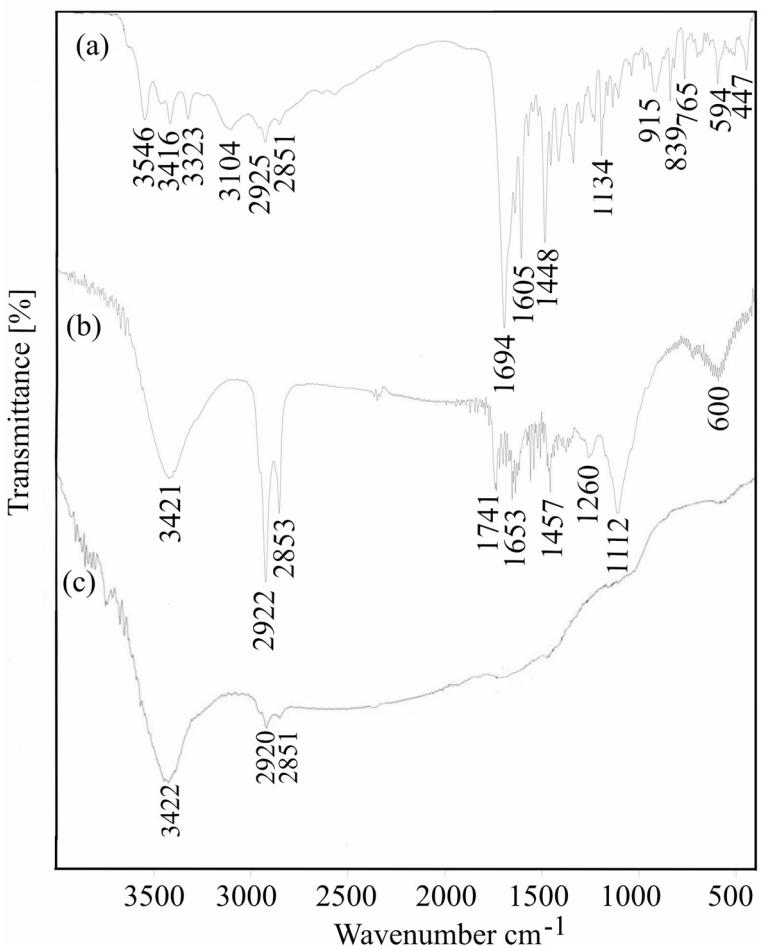

Fig. 3. Fourier transform infrared (FTIR) absorption spectra of (a) folic acid, (b) FA@Te NPs, and (c) Te NPs.

incorporation of diverse chemical functional groups onto nanoparticle surfaces[34]. Ameri et al.'s research utilized sodium alginate (a stabilizing agent) and Ascorbic acid (a reducing agent) in the microwave-assisted biosynthesis of palladium nanoparticles. Their findings, as evidenced by FTIR spectra, suggested a significant role of Ascorbic acid's functional group in the synthesis of Pd nanoparticles[35]. In another study, Shakibaie et al. used a water extract from *Eucalyptus camaldulensis* for the microwave-assisted production of Pt nanoparticles. They reported a correlation between the FTIR spectra of the dry extract and the resultant Pt nanoparticles, which they attributed to the binding of various extract compounds to the Pt nanoparticle surface during the formation process[48]. In the current investigation, a similarity was observed between Folic acid and FA@Te NPs in the fingerprint region of the FTIR spectrum (400 cm^{-1}-1500 cm^{-1}). This similarity suggests the presence of Folic acid on the surface of Te NPs. Quantitative analysis revealed that each milligram of the synthesized FA@Te NPs contained 37.1 ± 0.2 µg of folic acid. In comparison, other nanostructures such as umbelliprenin-coated Fe_3O_4 NPs and Fe_3O_4@piroctone olamine NPs, were found to contain 250 µg of umbelliprenin and 50 µg of piroctone olamine per milligram of dried nanoparticles, respectively[49]. It seems that the quantity of the coating process can be influenced by various factors, including the chemical structure of the coated compound, the type, size, shape, and synthesis method of the nanoparticles.

Antioxidant activity

This study aimed to evaluate the in vitro antioxidant activity of FA@Te NPs, Te NPs, and an Ascorbic acid solution by measuring their DPPH scavenging activity and reducing power (Fig. 4a, b). A range of concentrations between 20 µg/mL to 1280 µg/mL showed significantly greater scavenging activities with FA@Te NPs than with Te NPs ($p < 0.05$). Moreover, the study found that the scavenging effect of Ascorbic acid at concentrations ranging from 20 µg/mL to 160 µg/mL was significantly higher than the scavenging effect of FA@Te NPs and Te NPs ($p < 0.05$). The study found that the antioxidant activity of both FA@Te NPs and Te NPs was proportional to the amount administered. Previously, it has been reported that all types of folic acid (like folic acid, dihydrofolic acid, tetrahydrofolic acid, and methyl tetrahydrofolic acid) can scavenge DPPH radical and reduce Fe^{3+} to Fe^{2+} in the FRAP assay, where the lowest FRAP values and the highest IC_{50} value in the DPPH assay were obtained for Folic acid[50]. In another study, El-Borady et al. reported that folic acid-conjugated ZnO nanoparticles exhibited a higher DPPH scavenging activity (70%) compared to naked ZnO nanoparticles (64%) at the same concentration

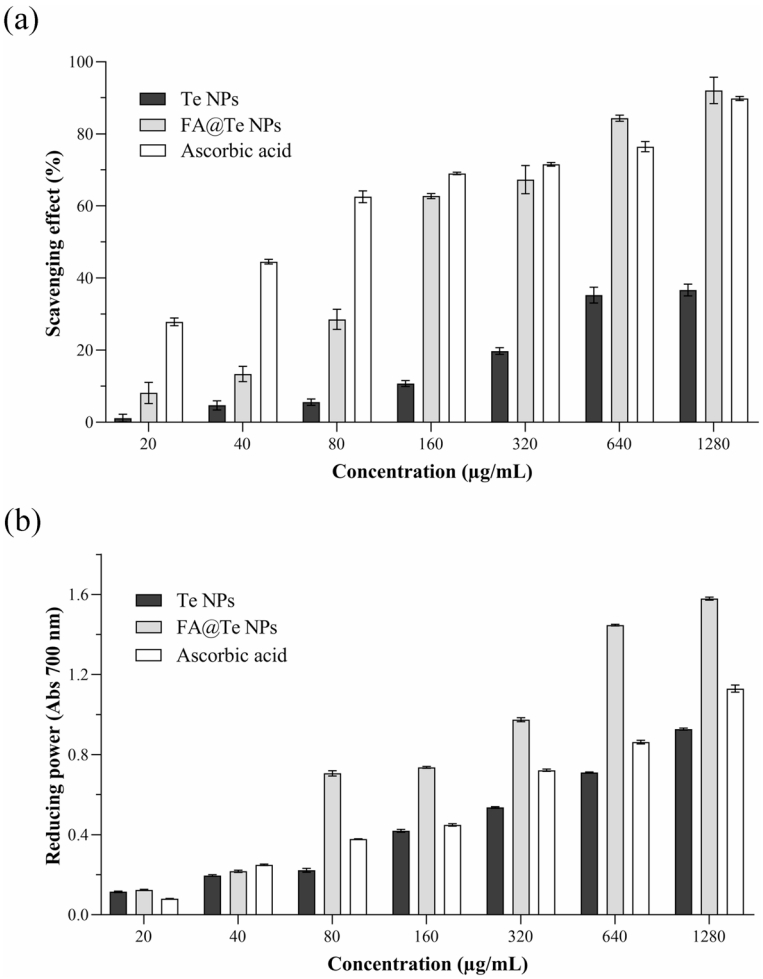

Fig. 4. The antioxidant activity of Te NPs, FA@Te NPs, and Ascorbic acid was evaluated using (a) the DPPH-free radical scavenging, and (b) the reducing power assay methods for different concentrations. Data represented as mean ± SD of three experiments.

of 300 µg/mL[51]. According to AbouAitah's results, conjugating folic acid to mesoporous silica particles as a nonocarrier for prodrugs resulted in a similar increase in radical scavenging activity in DPPH tests, which was often greater than free folic acid. This nanocarrier showed a synergistic enhancement in antioxidant capacity due to the carrier effects. Moreover, conjugation and loading of folic acid into nanoparticles have been shown to enhance antioxidant activity[52]. In another research, biogenic tellurium nanorods (22 nm in diameter) exhibited significant antioxidant activity by scavenging DPPH radicals with an IC50 value of 24.9 µg/mL. Moreover, these nanorods showed stronger reducing power compared to potassium tellurite, indicating a higher electron-donating ability[53].

The reducing power of FA@Te NPs, Te NPs, and Ascorbic acid solution was measured by reducing Fe^{3+} to Fe_{2+} ions (Fig. 4b). The reduction power of FA@Te NPs was significantly greater than that of Te NPs and Ascorbic acid at concentrations from 80 to 1280 µg/mL ($p < 0.05$). Ascorbic acid had significantly higher reducing power than Te NPs at concentrations from 40 to 1280 µg/mL ($p < 0.05$) (Fig. 4b). The enhanced reducing power activity of FA@Te NPs might be ascribed to their extensive surface area or their specific chemical structure. The elevated reducing power activity of FA@Te NPs could be linked to the chemical structure present on the nanoparticle surface or the nanoparticle's large surface area, which has the potential to convert Fe^{3+} ions. It has been previously reported that insoluble Zn NPs (30–80 nm), prepared by microwave irradiation, exhibit a comparable influence, demonstrating a higher reducing power activity than that of soluble Zn^{2+} ions[54].

The hemolytic properties of NPs

Based on the data in Fig. 5a, the study evaluated the hemolysis (destruction of red blood cells) caused by FA@Te NPs and Te NPs at varying concentrations. The hemolytic assay revealed that FA@Te nanoparticles (NPs) exhibited a notably elevated hemolytic potential (HP) compared to Te NPs at concentrations ranging from 20 to 40 µg/mL ($p < 0.05$). Conversely, at concentrations spanning from 160 to 1280 µg/mL, Te NPs demonstrated a significantly greater hemolytic potential (HP) than FA@Te NPs ($p < 0.05$). According to the ASTM F756-08 standard, substances with a hemolysis rate (HR) of less than 2% are classified as non-hemolytic, whereas

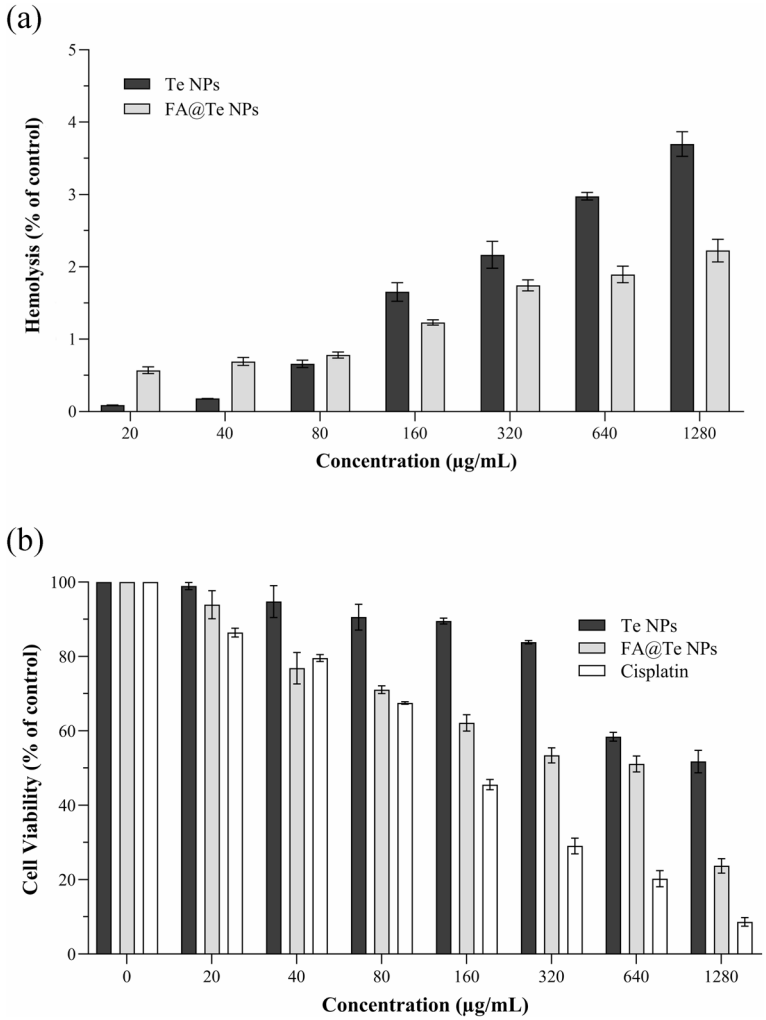

Fig. 5. In vitro hemolytic assay of Te NPs and FA@Te NPs (a), and Cytotoxicity effect of Te NPs, FA@Te NPs, and Cisplatin on HeLa cell line using MTT assay after 24 h incubation (b). All data are represented as mean ± SD of three experiments on different days.

biomaterials can have an HR of up to 5%[55,56]. Schiar et al. (2009) proposed that the hemolysis caused by tellurium compounds such as diphenyl ditelluride and naphthalene ditelluride is linked to the oxidation of intracellular glutathione (GSH). This oxidation leads to the production of free radicals (ROS), which in turn damage the red blood cells, causing their rupture. Their findings suggest that mechanism tellurium compounds induce oxidative stress inside cells by depleting protective thiols like GSH, resulting in hemolysis through radical-mediated membrane damage[57]. In the present study, the hemolytic properties (HP) of FA@Te NPs and Te NPs were found to be dose-dependent (Fig. 5a).

Cytotoxic activity

The cytotoxic properties of FA@Te NPs and Te NPs on HeLa cells were measured after 24 h of treatment (Fig. 5b). The necessary concentration for the death of half of the cells (IC_{50}) for HeLa cells treated (24 h) with FA@Te NPs, Te NPs, and Cisplatin was calculated to be 767.6 ± 8.8 µg/mL, 1399.5 ± 5.2 µg/mL, and 142.7 ± 4.6 µg/mL, respectively. In concentrations ranging from 20 to 80 µg/mL, FA@Te NPs exhibited significantly greater cytotoxic effects on HeLa cells than Te NPs ($p < 0.05$). Moreover, Cisplatin also caused significantly more toxicity on HeLa cells when applied at concentrations between 80 and 1280 µg/mL compared to FA@Te NPs and Te NPs ($p < 0.05$).

Fadhikeh et al. reported that the IC_{50} of Te NPs (45 nm, prepared using a tellurite potassium solution in the presence of lactose) for CHO cell, EJ138 cell line, and 4T1 cell line treated for 48 h was found to be 50.5 µg/mL, 29.6 µg/mL, and 7.4 µg/mL respectively. Additionally, when breast cancer-bearing mice were injected with 400 µg of Te NPs three times a week, they lived longer and experienced significant inhibition in tumor development compared to the control mice[58]. Vernet et al. reported that The IC_{50} of green-synthesized tellurium nanowires on HDF and melanoma cells were 70 µg/mL and 16.4 µg/mL, respectively[59]. In a study focusing on other tellurium-containing nanostructures, such as TeO_2 NPs, it was found that a concentration of 160 µg/mL of these nanoparticles was highly toxic to Human Pulmonary Alveolar Epithelial (HPAEpiC) and peripheral blood cells. Additionally, these nanoparticles did not exhibit antioxidant activity. However, it was observed that higher

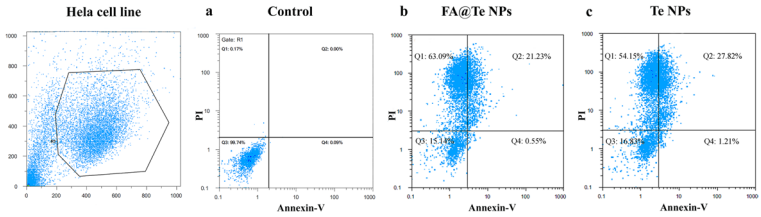

Fig. 6. Characteristic flow cytometry of HeLa cells exposed to nanoparticles at IC50 concentration. The numbers at the bottom right quadrant of each dot plot represent the percentage of cells in early apoptosis (annexin V-positive, PI-negative). Numbers at the top right quadrant represent the percentage of cells in late apoptosis and/or secondary necrosis (annexin V-positive, 7-AAD-positive) patterns. (a) Control, (b) treated with FA@Te NPs, (c) treated with Te NPs.

concentrations of the TeO_2 NPs could induce cytotoxic and pro-oxidant effects on both cell types[60]. It seems that several factors can affect the toxicity of cells treated with Te-containing nanostructures, including the shape, size, chemical composition, and nanoparticle preparation method.

Te-containing compounds have been found to induce neurodegeneration by establishing strong interactions with mitochondrial enzymes and proteins via the sulfhydryl group of cysteine, resulting in the modification and decreased abundance of the mitochondrial selenoprotein glutathione peroxidase, which plays a crucial role in regulating oxidative stress[61]. Given the similarity of tellurium to selenium, tellurium can also interact with selenoenzymes, such as glutathione peroxidase, leading to a decline in cellular redox modulatory activities and the onset of oxidative stress conditions that mediate cellular damage[62]. This imbalance in the protective mechanism of antioxidants can result in damage to cellular molecules, including DNA, proteins, and lipids, ultimately leading to cell death[62]. The compound, ammonium-trichloro [dioxoethyleneO, O'] tellurate, also known as AS101, has been demonstrated to inhibit the enzymatic activity of caspase-1, which is responsible for the maturation of pro-inflammatory cytokines IL-18 and IL-1β[63]. Specifically, treatment with AS101 has been found to decrease the levels of mature IL-18 and IL-1β in peripheral blood mononuclear cells (PBMCs) and HaCat keratinocytes, which are implicated in various inflammatory disorders. Furthermore, AS101 has been shown to stimulate the secretion of the anti-inflammatory cytokine IL-10 in an autocrine/paracrine manner in a variety of primary human cell cultures and suppress cell proliferation by antagonizing IL-10-mediated Stat3 phosphorylation and Bcl-2 expression[63]. Rocha et al. reported that two tellurium-containing Azidothymidine derivatives, with IC_{50} values of 24.95 and 21.61 µM, demonstrated selective cytotoxicity towards breast cancer cells and caused tumor cell cycle arrest in the MDA-MB-231 human breast tumor cell line[64]. The exact mechanism of Te NP cytotoxicity is not yet fully understood, but it is believed to be linked to its ability to bind to cellular proteins and DNA, leading to oxidative and DNA damage, and ultimately resulting in cell death via mitochondrial-dependent pathways[65]. Moreover, the biocompatibility of biogenic Te NPs is thought to be determined by the type of capping biomolecules[66].

Effect of nanoparticles on cell apoptosis

HeLa cells were stained with annexin V-FITC and PI as phosphatidylserine and DNA staining residues, respectively, and subjected to flow cytometry to determine the proportion of live, apoptotic, and necrotic cells. In flow cytometry images, the upper left quadrants (necrotic cells) and upper right quadrants (late-stage apoptosis) show the percentage of dead cells. The lower left quadrants (viable cells) and the lower right quadrants (early apoptosis) show the percentage of live cells (Fig. 6). The cell viability of the gated control group in Q3 quadrant was almost 99.74% (Fig. 6a) during the 24 h of culture; nevertheless, in cultures treated with IC_{50} concentrations of FA@Te NPs (Fig. 6b) and Te NPs (Fig. 6c) the cell viability was found to have decreased to 15.14%, and 16.83%, respectively. However, the percentage of necrotic cells in the Q1 quadrant was increased from 0.17% (Fig. 6a) to 63.09% and 54.15% for HeLa cells treated with FA@Te NPs (Fig. 6b) and Te NPs (Fig. 6c), respectively. As shown in Fig. 6a, a significant percentage of cells was shifted to late apoptosis or necrosis following treatment (24 h) with IC_{50} concentration of FA@Te NPs (767.6 µg/mL) and Te NPs (1399.5 µg/mL).

Treatment with various Te compounds has been observed to trigger both apoptosis and necrosis. It has been shown that exposure to Diphenyl ditelluride (DPDT) induces apoptosis and promotes necrosis in the presence of tellurium tetrachloride ($TeCl_4$)[67]. Necrosis was observed in Schwann cells, which produce a myelin sheath around axons in the peripheral nervous system, upon exposure to Te[68]. In the case of other tellurium-containing nanostructures, it has been observed that biogenic Tellurium nanorods (185 nm in length and 22 nm in width) primarily trigger late apoptosis or necrosis at the IC_{50} concentration. This occurs without influencing the activities of caspase-3 in the PC12 cell line. Moreover, these Te nanorods have been found to decrease glutathione levels, increase malondialdehyde levels, and also diminish the activities of superoxide dismutase and catalase in the PC12 cell line[69]. Shahverdi et al. previously reported that folic acid-coated selenium nanoparticles (Se NPs) exhibited higher cytotoxicity in the 4T1 breast cancer cell line compared to uncoated Se NPs, and these nanoparticles also resulted in a more significant reduction in tumor growth rate in cancerous mice[70]. In a separate study, Pi et al. found that MCF-7 cells could internalize folic acid-coated metalloid nanoparticles, such as FA-Se NPs (70 nm), via endocytosis through the folate receptor[71]. Following internalization, these nanoparticles initiated mitochondria-dependent apoptosis, nucleolar damage, cell cycle arrest, cytoskeleton disorganization, and alterations in cell membrane morphology in MCF-7 cells[71]. Indeed, the exact mechanisms

underlying the cytotoxic effects of FA@Te NPs have not been fully understood, and further research is needed to elucidate these mechanisms.

Conclusion

In summary, the study successfully synthesized and characterized FA@Te nanoparticles using microwave irradiation of a K2TeO3 solution containing folic acid. The UV-Vis absorption spectra, SEM micrographs, particle size distribution patterns, EDX, XRD, and FTIR analyses provided valuable insights into the physical and chemical properties of these nanoparticles, confirming the successful synthesis of Te nanoparticles and suggesting the presence of folic acid on their surface. The results demonstrated that FA@Te NPs exhibited significantly greater scavenging activities than Te NPs across a range of concentrations. Furthermore, the antioxidant activity of both FA@Te NPs and Te NPs was found to be dose-dependent. The study also highlighted the superior reducing power of FA@Te NPs, which could be attributed to their extensive surface area or specific chemical structure. In addition, the hemolytic properties of FA@Te NPs and Te NPs were evaluated, revealing a dose-dependent hemolytic potential. This study has successfully evaluated the cytotoxic properties of FA@Te NPs and Te NPs on HeLa cells, revealing that FA@Te NPs exhibited significantly greater cytotoxic effects at certain concentrations. The study also found that the cytotoxicity of these nanoparticles was dose-dependent. The results revealed a significant decrease in cell viability and an increase in necrotic and late apoptotic HeLa cells following treatment with IC_{50} concentrations of FA@Te NPs and Te NPs.

According to the enhanced antioxidant performance of FA@Te NPs in DPPH and FRAP results, it can be suggested that the folic acid functionalization not only targets cancer cells, such as HeLa, more specifically by recognizing folate receptors, but also enhances antioxidative defense through effective scavenging of free radicals and iron reducing power at a dose-dependent rate. However, the exact mechanisms underlying the cytotoxic effects of FA@Te NPs remain unclear, highlighting the need for further research to fully understand these mechanisms.

Data availability

The datasets used and analyzed during this study are available from the corresponding author on reasonable request.

Received: 23 June 2025; Accepted: 8 December 2025
Published online: 18 December 2025

References

1. Zhu, H. et al. Progress in the synthesis and application of tellurium nanomaterials. *Nanomaterials* **13**, 2057. https://doi.org/10.3390/nano13142057 (2023).
2. Sári, D. et al. Tellurium and nano-tellurium: medicine or poison? *Nanomater. (Basel Switzerl.)* **14**, 2563. https://doi.org/10.3390/nano14080670 (2024).
3. Ao, B. et al. Synthesis of tellurium nanoparticles using Moringa Oleifera extract, and their antibacterial and antibiofilm effects against bacterial pathogens. *Microorganisms* **12**, 256 (2024).
4. Matharu, R. K., Charani, Z., Ciric, L., Illangakoon, U. E. & Edirisinghe, M. Antimicrobial activity of tellurium-loaded polymeric fiber meshes. *J. Appl. Polym. Sci.* **135**, 46368. https://doi.org/10.1002/app.46368 (2018).
5. Domínguez-Álvarez, E. et al. Selenium and tellurium in the development of novel small molecules and nanoparticles as cancer multidrug resistance reversal agents. *Drug Resist. Updates*. **63**, 100844. https://doi.org/10.1016/j.drup.2022.100844 (2022).
6. Yossipof, T. E. et al. Tellurium compounds prevent and reverse type-1 diabetes in NOD mice by modulating α4β7 integrin activity, IL-1β, and T regulatory cells. *Front. Immunol.* **10**, 979. https://doi.org/10.3389/fimmu.2019.00979 (2019).
7. Halpert, G. et al. The tellurium-based immunomodulator, AS101 ameliorates adjuvant-induced arthritis in rats. *Clin. Exp. Immunol.* **203**, 375–384. https://doi.org/10.1111/cei.13553 (2021).
8. Sahoo, B. M. et al. Synthesis and application of organotellurium compounds. *Phys. Sci. Rev.* https://doi.org/10.1515/psr-2021-0105 (2022).
9. Liu, Y. H. et al. A tellurium-based small compound ameliorates tumor metastasis by downregulating heparanase expression. *J. Cancer*. **15**, 5308–5317. https://doi.org/10.7150/jca.96001 (2024).
10. Ajideh, R. et al. The cytotoxicity of tellurium nanoparticles on different cell lines and their in vivo anticancer effects in an animal model. *Middle East. J. Cancer*. **14**, 17–27. https://doi.org/10.30476/mejc.2022.91698.1630 (2023).
11. Chiaverini, L., Marzo, T. & La Mendola, D. AS101: an overview on a leading tellurium-based prodrug. *Inorg. Chim. Acta*. **540**, 121048. https://doi.org/10.1016/j.ica.2022.121048 (2022).
12. Medina Cruz, D. et al. Citric juice-mediated synthesis of tellurium nanoparticles with antimicrobial and anticancer properties. *Green. Chem.: Int. J. green. Chem. Resource : GC*. **21**, 1982–1988. https://doi.org/10.1039/C9GC00131J (2019).
13. Li, T. et al. Nanostructures and catalytic atoms engineering of tellurium-based materials and their roles in electrochemical energy conversion. *SmartMat* **4**, e1142. https://doi.org/10.1002/smm2.1142 (2023).
14. Li, C. et al. Advances of bioactive tellurium nanomaterials in anti-cancer phototherapy. *Mater. Adv.* https://doi.org/10.1039/D2MA00318J (2022).
15. Poulose, A. C. et al. Multifunctional Cu2 – xTe nanocubes mediated combination therapy for multi-drug resistant MDA MB 453. *Sci. Rep.* **6**, 35961. https://doi.org/10.1038/srep35961 (2016).
16. Morena, A. G., Bassegoda, A., Hoyo, J. & Tzanov, T. Interfaces. Hybrid tellurium–lignin nanoparticles with enhanced antibacterial properties. *ACS Appl. Mater.* **13**, 14885–14893. https://doi.org/10.1021/acsami.0c22301 (2021).
17. Kang, S., Gil, Y. G., Yim, G., Min, D. H. & Jang, H. Osmium–Tellurium nanozymes for pentamodal combinatorial cancer therapy. *ACS Appl. Mater. Interfaces*. **13**, 44124–44135. https://doi.org/10.1021/acsami.1c14201 (2021).
18. Guo, Z. et al. Versatile biomimetic cantharidin-tellurium nanoparticles enhance photothermal therapy by inhibiting the heat shock response for combined tumor therapy. *Acta Biomater.* **110**, 208–220. https://doi.org/10.1016/j.actbio.2020.03.028 (2020).
19. Yang, T. et al. Bifunctional tellurium nanodots for photo-induced synergistic cancer therapy. *ACS Nano*. **11**, 10012–10024. https://doi.org/10.1021/acsnano.7b04230 (2017).
20. Ly, P. D. et al. Recent advances in surface decoration of nanoparticles in drug delivery. *Front. Nanotechnol.* **2024**, 6. https://doi.org/10.3389/fnano.2024.1456939 (2024).
21. Jurczyk, M. et al. Single- versus dual-targeted nanoparticles with folic acid and biotin for anticancer drug delivery. *Pharmaceutics* **13**, 253. https://doi.org/10.3390/pharmaceutics13030326 (2021).

22. Premjit, Y., Pandey, S. & Mitra, J. Recent trends in folic acid (Vitamin B9) encapsulation, controlled release, and mathematical modelling. *Food Reviews Int.* **39**, 5528–5562. https://doi.org/10.1080/87559129.2022.2077361 (2023).
23. Young, O. et al. Folate receptor as a biomarker and therapeutic target in solid tumors. *Curr. Probl. Cancer*. **47**, 100917. https://doi.org/10.1016/j.currproblcancer.2022.100917 (2023).
24. Varaganti, P., Buddolla, V., Lakshmi, B. A. & Kim, Y. J. Recent advances in using folate receptor 1 (FOLR1) for cancer diagnosis and treatment, with an emphasis on cancers that affect women. *Life Sci.* **2023**, 121802. https://doi.org/10.1016/j.lfs.2023.121802 (2023).
25. Norton, N. et al. Folate receptor alpha expression associates with improved disease-free survival in triple negative breast cancer patients. *Npj Breast Cancer*. **6**, 4. https://doi.org/10.1038/s41523-020-0147-1 (2020).
26. Hijaz, M. et al. Folic acid tagged nanoceria as a novel therapeutic agent in ovarian cancer. *BMC Cancer*. **16**, 220. https://doi.org/10.1186/s12885-016-2206-4 (2016).
27. Gomaa, S., Nassef, M., Tabl, G., Zaki, S. & Abdel-Ghany, A. Doxorubicin and folic acid-loaded zinc oxide nanoparticles-based combined anti-tumor and anti-inflammatory approach for enhanced anti-cancer therapy. *BMC Cancer*. **24**, 1–16. https://doi.org/10.1186/s12885-023-11714-4 (2024).
28. Rajana, N. et al. Targeted delivery and apoptosis induction of CDK-4/6 inhibitor loaded folic acid decorated Lipid-Polymer hybrid nanoparticles in breast cancer cells. *Int. J. Pharm.* **2024**, 123787. https://doi.org/10.1016/j.ijpharm.2024.123787 (2024).
29. Pal, M. et al. Folate-assisted targeted photocytotoxicity of red-light-activable iron (iii) complex co-functionalized gold nanoconjugates (Fe@ FA-AuNPs) against HeLa and triple-negative MDA-MB-231 cancer cells. *Dalton Trans.* **53**, 2108–2119. https://doi.org/10.1039/D3DT03581F (2024).
30. Adhikari, A. R. & Chipara, M. A recent development trend in microwave radiation-based material engineering. *Polym. Bull.* **2024**, 1–20. https://doi.org/10.1007/s00289-023-05119-3 (2024).
31. Magdy, G., Aboelkassim, E., El-Domany, R. A. & Belal, F. Ultrafast one-pot microwave-assisted green synthesis of silver nanoparticles from Piper longum fruit extract as a sensitive fluorescent nanoprobe for carbamazepine and Risperidone in dosage forms and human plasma. *Microchem. J.* **197**, 109755. https://doi.org/10.1016/j.microc.2023.109755 (2024).
32. Khanam, B. R. et al. Gamma radiation-induced modifications in the physiochemical features of ZnO nanoparticles synthesized using microwave technique. *Ceram. Int.* **50**, 5552–5561. https://doi.org/10.1016/j.ceramint.2023.11.310 (2024).
33. Shakibaie, M. et al. Preparation of folic acid@Arsenic nanoparticles and evaluation of their antioxidant properties and cytotoxic effects. *Pharm. Nanatechnol.* https://doi.org/10.2174/2211738511666230507175710 (2023).
34. Shakibaie, M. et al. Microwave assisted biosynthesis of cadmium nanoparticles: characterization, antioxidant and cytotoxicity studies. *J. Cluster Sci.* **33**, 1877–1887. https://doi.org/10.1007/s10876-021-02107-3 (2022).
35. Ameri, A. et al. Rapid and facile microwave-assisted synthesis of palladium nanoparticles and evaluation of their antioxidant properties and cytotoxic effects against fibroblast-like (HSkMC) and human lung carcinoma (A549) cell lines. *Biol. Trace Elem. Res.* **197**, 132–140. https://doi.org/10.1007/s12011-019-01984-0 (2020).
36. Satarzadeh, N. et al. Facile microwave-assisted biosynthesis of arsenic nanoparticles and evaluation their antioxidant properties and cytotoxic effects: a preliminary in vitro study. *J. Cluster Sci.* **34**, 1831–1839. https://doi.org/10.1007/s10876-022-02356-w (2023).
37. Múzquiz-Ramos, E. M., Guerrero-Chávez, V., Macías-Martínez, B. I., López-Badillo, C. M. & García-Cerda, L. A. Synthesis and characterization of maghemite nanoparticles for hyperthermia applications. *Ceram. Int.* **41**, 397–402. https://doi.org/10.1016/j.ceramint.2014.08.083 (2015).
38. Forootanfar, H. et al. Microbial-assisted synthesis and evaluation the cytotoxic effect of tellurium nanorods. *Mater. Sci. Eng. C* **49**, 183–189. https://doi.org/10.1016/j.msec.2014.12.078 (2015).
39. Phae-Ngam, W., Kosalathip, V., Kumpeerapun, T., Limsuwan, P. & Dauscher, A. Preparation and characterization of tellurium nano-particles by long pulsed laser ablation. *Adv. Mater. Res.* **214**, 202–206. https://doi.org/10.4028/www.scientific.net/AMR.214.202 (2011).
40. Abed, N. N., El-Enain, A., Helal, I. M., Yosri, M. & E. E.-H. & Novel biosynthesis of tellurium nanoparticles and investigation of their activity against common pathogenic bacteria. *J. Taibah Univ. Med. Sci.* **18**, 400–412. https://doi.org/10.1016/j.jtumed.2022.10.006 (2023).
41. Barabadi, H., Kobarfard, F. & Vahidi, H. Biosynthesis and characterization of biogenic tellurium nanoparticles by using penicillium chrysogenum PTCC 5031: a novel approach in gold biotechnology. *Iran. J. Pharm. Res.: IJPR*. **17**, 87 (2018).
42. Iesari, F. et al. Characterization of Te nanoparticles synthesized by plasma processing. *Radiation Phys. Chem.* **175**, 108334. https://doi.org/10.1016/j.radphyschem.2019.05.024 (2020).
43. Hosseini, F., Lashani, E. & Moghimi, H. Simultaneous bioremediation of phenol and tellurite by Lysinibacillus sp. EBL303 and characterization of biosynthesized Te nanoparticles. *Sci. Rep.* **13**, 1243. https://doi.org/10.1038/s41598-023-28468-5 (2023).
44. Askar, M. A. et al. Amygdalin-folic acid-nanoparticles inhibit the proliferation of breast cancer and enhance the effect of radiotherapy through the modulation of tumor-promoting factors/ immunosuppressive modulators in vitro. *BMC Complement. Med. Ther.* **23**, 162. https://doi.org/10.1186/s12906-023-03986-x (2023).
45. Li, H. et al. Facile electrochemical synthesis of tellurium nanorods and their photoconductive properties. *Cryst. Res. Technol.* **47**, 1069–1074. https://doi.org/10.1002/crat.201200273 (2012).
46. Mousavi-Kamazani, M., Rahmatolahzadeh, R., Shobeiri, S. A. & Beshkar, F. Sonochemical synthesis, formation mechanism, and solar cell application of tellurium nanoparticles. *Ultrason. Sonochem.* **39**, 233–239. https://doi.org/10.1016/j.ultsonch.2017.04.031 (2017).
47. Rosales-Conrado, N., Gómez-Gómez, B., Matías-Soler, J., Pérez-Corona, M. T. & Madrid-Albarrán, Y. Comparative study of tea varieties for green synthesis of tellurium-based nanoparticles. *Microchem. J.* **169**, 106511. https://doi.org/10.1016/j.microc.2021.106511 (2021).
48. Shakibaie, M. et al. Rapid microwave-assisted biosynthesis of platinum nanoparticles and evaluation of their antioxidant properties and cytotoxic effects against MCF-7 and A549 cell lines. *3 Biotech.* **11**, 511. https://doi.org/10.1007/s13205-021-03007-z (2021).
49. Shakibaie, M. et al. Preparation and evaluation of the effect of Fe3O4@piroctone olamine magnetic nanoparticles on matrix metalloproteinase-2: a preliminary in vitro study. **61**, 676–682. https://doi.org/10.1002/bab.1231 (2014).
50. Gliszczyńska-Świgło, A. Folates as antioxidants. *Food Chem.* **101**, 1480–1483. https://doi.org/10.1016/j.foodchem.2006.04.022 (2007).
51. El-Borady, O. M. & El-Sayed, A. F. Synthesis, morphological, spectral and thermal studies for folic acid conjugated ZnO nanoparticles: potency for multi-functional bio-nanocomposite as antimicrobial, antioxidant and photocatalytic agent. *J. Mater. Res. Technol.* **9**, 1905–1917. https://doi.org/10.1016/j.jmrt.2019.12.022 (2020).
52. AbouAitah, K. et al. Folic acid-conjugated mesoporous silica particles as nanocarriers of natural prodrugs for cancer targeting and antioxidant action. *Oncotarget* **9**, 26466–26490. https://doi.org/10.18632/oncotarget.25470 (2018).
53. Shakibaie, M. et al. Antimicrobial and antioxidant activity of the biologically synthesized tellurium Nanorods; A preliminary in vitro study. *Iran. J. Biotechnol.* **15**, 268–276. https://doi.org/10.15171/ijb.1580 (2017).
54. Salari, Z. et al. Microwave-assisted biosynthesis of zinc nanoparticles and their cytotoxic and antioxidant activity. *J. Trace Elem. Med Biol.* **39**, 116–123. https://doi.org/10.1016/j.jtemb.2016.09.001 (2017).
55. Singh, N., Sahoo, S. K. & Kumar, R. Hemolysis tendency of anticancer nanoparticles changes with type of blood group antigen: an insight into blood nanoparticle interactions. *Mater. Sci. Eng.: C* **109**, 110645. https://doi.org/10.1016/j.msec.2020.110645 (2020).
56. Múzquiz-Ramos, E. M. et al. In vitro and in vivo biocompatibility of apatite-coated magnetite nanoparticles for cancer therapy. *J. Mater. Science: Mater. Med.* **24**, 1035–1041. https://doi.org/10.1007/s10856-013-4862-0 (2013).

57. Schiar, V. P. P. et al. Human erythrocyte hemolysis induced by selenium and tellurium compounds increased by GSH or glucose: a possible involvement of reactive oxygen species. *Chemico-Biol. Interact.* **177**, 28–33. https://doi.org/10.1016/j.cbi.2008.10.007 (2009).
58. Ajideh, R. et al. The cytotoxicity of tellurium nanoparticles on different cell lines and their in vivo anticancer effects in an animal model. *J. Middle East. J. Cancer.* **14**, 17–27 (2023).
59. Vernet Crua, A. et al. Comparison of cytocompatibility and anticancer properties of traditional and green chemistry-synthesized tellurium nanowires. *Int. J. Nanomed.* **2019**, 3155–3176. https://doi.org/10.2147/IJN.S175640 (2019).
60. Aydin, N., Arslan, M. E., Sonmez, E. S. & Turkez, H. Cytotoxicity analysis of tellurium dioxide nanoparticles on cultured human pulmonary alveolar epithelial and peripheral blood cell cultures. *Biomed. Res. India*. **28**, 3300–3304 (2017).
61. Vávrová, S., Struhárňanská, E., Turňa, J. & Stuchlík, S. Tellurium A rare element with influence on prokaryotic and eukaryotic biological systems. *Int. J. Mol. Sci.* **22**, 256. https://doi.org/10.3390/ijms22115924 (2021).
62. Olawale, F., Oladimeji, O., Ariatti, M. & Singh, M. Emerging roles of green-synthesized chalcogen and chalcogenide nanoparticles in cancer theranostics. *J. Nanatechnol.* **2022**, 1–18. https://doi.org/10.1155/2022/6176610 (2022).
63. Seng, H. L. & Tiekink, E. R. Anti-cancer potential of selenium-and tellurium-containing species: opportunities abound! *Appl. Organomet. Chem.* **26**, 655–662. https://doi.org/10.1002/aoc.2928 (2012).
64. Rocha, A. M. O. et al. Evaluation of the effect of synthetic compounds derived from Azidothymidine on MDA-MB-231 type breast cancer cells. *Bioorg. Med. Chem. Lett.* **30**, 127365. https://doi.org/10.1016/j.bmcl.2020.127365 (2020).
65. Huang, W. et al. Triangle-shaped tellurium nanostars potentiate radiotherapy by boosting checkpoint Blockade immunotherapy. *Matter* **3**, 1725–1753. https://doi.org/10.1016/j.matt.2020.08.027 (2020).
66. Huang, W., Wu, H., Li, X. & Chen, T. Facile One-Pot synthesis of tellurium nanorods as antioxidant and anticancer agents. *Chemistry–An Asian J.* **11**, 2301–2311. https://doi.org/10.1002/asia.201600757 (2016).
67. Vij, P. & Hardej, D. J. E. T. Evaluation of tellurium toxicity in transformed and non-transformed human colon cells. *Environ. Toxicol. Pharmacol.* **34**, 768–782. https://doi.org/10.1016/j.etap.2012.09.009 (2012).
68. Berciano, M. T. et al. Necrosis of Schwann cells during tellurium-induced primary demyelination: DNA fragmentation, reorganization of splicing machinery, and formation of intranuclear rods of actin. *J. Neuropathol. Exp. Neurol.* **58**, 1234–1243. https://doi.org/10.1097/00005072-199912000-00004 (1999).
69. Shakibaie, M. et al. Cytotoxicity investigations of biogenic tellurium nanorods towards PC12 cell line. *IET Nanobiotechnol.* **12**, 1144–1149. https://doi.org/10.1049/iet-nbt.2018.5137 (2018).
70. Shahverdi, A. R. et al. Characterization of folic acid surface-coated selenium nanoparticles and corresponding in vitro and in vivo effects against breast cancer. *Arch. Med. Res.* **49**, 10–17. https://doi.org/10.1016/j.arcmed.2018.04.007 (2018).
71. Pi, J. et al. Pathway of cytotoxicity induced by folic acid modified selenium nanoparticles in MCF-7 cells. *Appl. Microbiol. Biotechnol.* **97**, 1051–1062. https://doi.org/10.1007/s00253-012-4359-7 (2013).

Acknowledgements

We thank the Pharmaceutical Sciences and Cosmetic Products Research Center, Institute of Pharmaceutical Sciences, Kerman University of Medical Sciences, (Kerman, Iran) for their laboratory and equipment support.

Author contributions

Writing-original draft: M.S; Acquisition of samples and data: N.S, S.R, and F.J; methodology: N.S; M.A; validation: H.F; formal analysis: M.A, M.S; Statistical analysis: F.J; Final reviewing and editing: M.S., M.A, and H.F; The authors have read and agreed to the published version of the manuscript.

Funding

Research reported in this publication was also supported by the Elite Researcher Grant Committee (Research Ethics Committees Certificate, IR.NIMAD.REC.1403.004) under award number from the National Institutes for Medical Research Development (NIMAD, 4002332), Tehran, Iran.

Competing interests

The authors declare no competing interests.

Additional information

Correspondence and requests for materials should be addressed to M.S. or M.A.-S.